WP15ER-CPR(18) 19174

M Chernyshova et al.

2D GEM based imaging detector readout capabilities from perspective of intense soft X-ray plasma radiation

Preprint of Paper to be submitted for publication in Proceeding of 18th Topical Conference on High Temperature Plasma Diagnostics (HTPD)

This work has been carried out within the framework of the EUROfusion Consortium and has received funding from the Euratom research and training programme 2014-2018 under grant agreement No 633053. The views and opinions expressed herein do not necessarily reflect those of the European Commission.

2D GEM based imaging detector readout capabilities from perspective of intense soft X-ray plasma radiation[a)]

M. Chernyshova,[1,b)] T. Czarski,[1] K. Malinowski,[1] Y. Melikhov,[3] G. Kasprowicz,[2] E. Kowalska-Strzęciwilk,[1] P. Linczuk,[1,2] A. Wojeński,[2] and R. D. Krawczyk[2]

[1]*Institute of Plasma Physics and Laser Microfusion, 23 Hery str., 01-497 Warsaw, Poland*
[2]*Warsaw University of Technology, Institute of Electronic Systems, Nowowiejska 15/19, 00-665 Warsaw Poland*
[3]*School of Engineering, Cardiff University, CF24 3AA, Cardiff, United Kingdom*

(Presented XXXXX; received XXXXX; accepted XXXXX; published online XXXXX)

A detecting system based on the Gas Electron Multiplier (GEM) technology is considered for tokamak plasma radiation monitoring. In order to estimate its capabilities in processing and recording intense photon flux (up to ~0.1 MHz/mm^2), the imaging effectiveness of GEM detectors was tested with different patterned anode planes (i.e. different signal readouts): three structures with interconnected electrodes (XY squared, XY rectangular, and UXV) and a simple hexagonal readout structure. It was found that under intense photon flux, all the readouts fail to account for a considerable amount of the incoming signals due to mostly photon position determination ambiguity and overlapped signals. Analysis of the signals that can be used to determine photon position and energy unambiguously showed that the UXV readout structure is more effective among the readouts with interconnected electrodes. Along with similar spatial resolution and accuracy, the UXV based layout could be considered as a quite promising base of the interconnected anode electrodes configuration, keeping in mind that the photon rate capability has to be improved for the final application.

I. INTRODUCTION

Tokamak plasma imaging in the Soft X-Ray (SXR) region can provide valuable information on particle transport and magnetic configuration leading to a safe and effective operation of the tokamak. As metallic impurities released to the plasma volume from metallic parts (e.g., tungsten containing walls machines) contaminate plasma and due to interplay between particle transport and MagnetoHydroDynamics (MHD) activity, this might lead to impurities accumulation, and, eventually, to disruption of the thermonuclear fusion reaction.

A detecting system that consists of several Triple-GEM (Gas Electron Multiplier)[1] detectors is currently being designed and developed for standard 2D tomography of soft X-ray radiation (~2–17 keV) coming from a tokamak plasma[2-7]. In order to provide spatial distribution of X-ray emission during many plasma processes, such an imaging system would consist of a set of two 1D GEM cameras in a common poloidal cross-section (standard tomography). Adding a complementary toroidal 2D GEM camera the additional 3D information can be used to constrain 2D tomography, do direct imaging, test MHD simulations (synthetic diagnostic) or to explore 3D tomography. Such a detecting system allows energy discrimination of the incident absorbed photons as well as good spatial resolution (i.e., localization of their position on the detector readout pads). Moreover, its advantages refer also to compactness, good temporal resolution, and better neutron resilience than the existing systems.

One of the remarkable properties of the GEM based detector is a spatial separation of the processes of charge transfer/amplification and its collection (i.e. signal reading). Extensive studies have been made to optimize response of a GEM detector. Physical dimensions and geometry of foils and holes[8,9], voltages to generate an optimal electric field distribution[10], composition and flow rates of working gas mixture are among such studies. A micro patterned readout is another important element of a GEM camera. It is responsible for effective extraction of the accumulated signal from the electron cloud and its correct transfer into further electronics. The choice of the readout plane geometry is of a high significance for spatially resolved capabilities of the detector. In this paper, the limits of applicability of several readout structures are tested, both at intense photon rates and at maximal achievable spatial resolution aiming to define their suitability for plasma radiation imaging by GEM detector.

II. READOUT STRUCTURE EFFECT ON DETECTOR CAPABILITIES

[a)]Published as part of the Proceedings of the 22nd Topical Conference on High-Temperature Plasma Diagnostics (HTPD 2018) in San Diego, California, USA.
[b)]Author to whom correspondence should be addressed: maryna.chernyshova@ipplm.pl.

A. Experimental details

The model triple-GEM detector was used in these studies. Each GEM foil is an insulating polymer film (Kapton®) with a thickness of 50 μm with a regular pattern of double conical holes with 50/70 μm inner/outer diameters. The distance between the holes was 140 μm producing a high density of ~100 mm^{-2}. As cladding, a thin layer (5 μm) of copper was coated on both sides of the film. The camera was filled with the Ar/CO_2 mixture at the ratio of 70/30%. During the operation, the flow rate was 50 ml/min. The readout pixel structure (anode) was connected to the readout electronics[11-13], which was able to provide a signal rate up to 2.5 MHz per individual channel.

The X-rays used in these studies were generated by an X-ray generator operated at 5 or 6 kV high voltage, producing ~5 or 6 keV photons, correspondingly, whose intensity was changed by the applied current in the range of 0.5-100 μA. The detecting surface was exposed to radiation either through a long (50 mm) collimator of 1.1 mm diameter, spot of Ø10 mm or without any collimator for an object imaging.

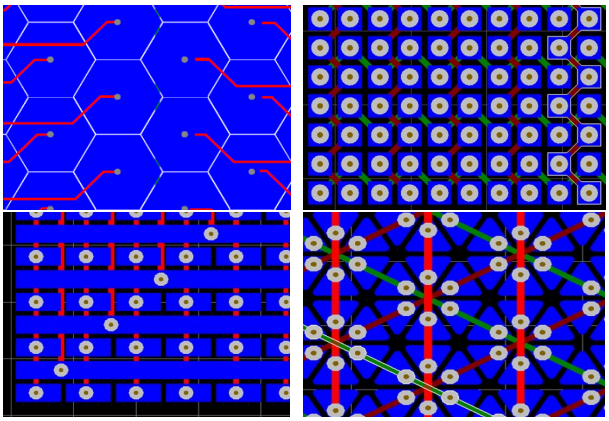

FIG. 1. (color online) Layouts of anode pad structures (blue areas) and their interconnection (bright red, green and dark red segments) for independent electronics channels: (a) the simplest structure with hexagonal subpixels; and structures with interconnected electrodes: (b) XY configuration with square subpixels; (c) XY configuration with rectangular subpixels; (d) UXV configuration with triangle subpixels.

As a readout structure imposes number of the electronics channels, in the case of large detecting surface (typical for tokamak applications), it is always a compromise between good spatial resolution along with unambiguity of photon position reconstruction and minimization of electronics elements. Therefore, in this work we consider different layouts for ~100x100 mm^2 detecting surface to optimize both parameters. Four readout geometries were tested to investigate their spatial resolution and abilities to process intense photon flux that is crucial for tokamak plasma imaging diagnostics. FIG. 1 shows the investigated anode pad structures and their interconnection to independent electronics channels. The first, simplest structure contains pads of [16x16] hexagons of 2.696 mm leg at 4.68 mm pitch connected independently to the individual electronics channels. Two XY readout structures have squared and rectangular [64x64] pixels, respectively, with 128 measurement channels each, both of 0.5 mm pitch. The squared pixels have 0.4 mm sides and are interconnected in a zigzag way either in x or y direction, whilst rectangular are independent pixels of either 0.4x0.9 mm^2 (connected together along Y coordinate) or 0.4x100 mm^2 (along X coordinate). Finally, UXV readout has 192 measurement channels for 18432 triangle sub-pixels connected along three symmetrical directions forming a hexagonal net (note that three-axis coordinate system has to be used here with axes at 60º with respect to each other). It has 1.006 mm side triangles of 1.661 mm hexagon pitch.

B. Detector signal processing

The choice of the readout plane geometry is crucial for spatially resolved capabilities of the detector. When measuring coordinates of track particles, anode is usually in a form of a single layer or double layer strip structure[14], allowing one-dimensional or two-dimensional extraction of information, respectively. In some cases, the anode of the GEM detector is in the form of pads/pixels[15], to ensure maximum resolution for multi-track events. This is due to the fact that when a photoabsorption event of a single photon occurs, it eventually results in a charge cloud that arrives onto the anode covering one or several pixels (that is called a charge cluster), depending on the readout geometry. FIG. 2 illustrates a dependence of a charge cluster size on UXV readout plane on photon energy; an example of its identification in case of a charge spread over four pixels for hexagonal readout is on the inset in FIG. 2. Here, for 2D imaging purposes and Cartesian representation of the data, the original hexagon was assigned to two rectangles (for more details see[16]). The identification of a charge cluster is unique for all the examined anode structures (for hexagonal and UXV structure see[16,17]; simpler XY readouts were treated in the similar way; for square pixels see[18]) allowing identification of number of pixels involved. An analysis of their geometric positions (coordinates (x,y) marked on the inset of FIG. 2) enables an estimation of the cluster size as a function of photon energy (i.e. generated detector charge) shown in FIG. 2, whereas the total cluster charge corresponds to the absorbed photon energy.

The detector signals imaging was prepared assuming that the pixel charge collected for a single photon absorption relates to a probability of photon absorption on the related detecting surface. Therefore, charge cluster position is defined by relative values of the pixel charges forming a given cluster. The cluster charge identification starts from searching (at a certain moment of time) through the channel charges table for the successive maximal

charge enclosed within its rectangular environment ([*X*,*Y*] area marked in the inset in FIG. 2). This cluster is required to be surrounded by "zero-charge" neighbors (see the inset in FIG. 2). The total cluster charge Q, is therefore calculated as a sum of all partial charges q_i within the selected area. The cluster position is identified using standard weighing approach: each pixel contributes with its own relative weight q_i/Q to the position.

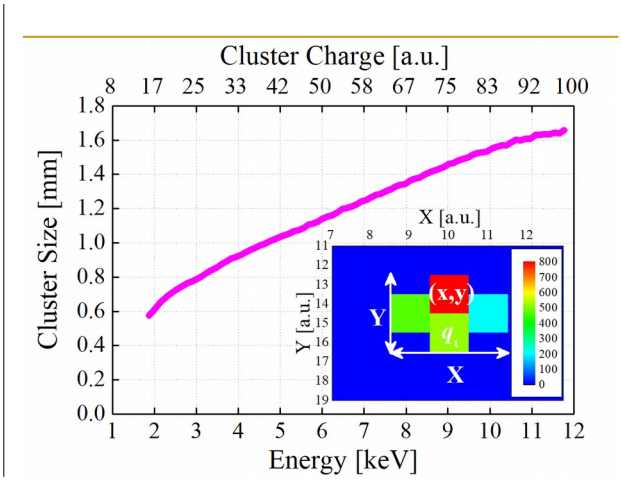

FIG. 2. (color online) Identification of the charge cluster size in the whole energy/charge range of detector operation using the UXV readout plane. Inset shows an example of a charge spread on the hexagonally patterned readout plane as a result of a photoabsorption of a single photon. Different colors represent different amount of charge on a particular pixel. Each hexagon is presented by two rectangles to account for neighboring hexagons relative shift in the vertical direction (for more details see[16]). Four charges (with (*x*,*y*)

Since the main idea of the detector is to detect multiple events, the algorithms to uniquely distinguish sequential individual events during data acquisition have to be employed. Due to straightforward construction, these algorithms are relatively simple in XY rectangular and square structures (FIG. 1 (b), (c)) as there are only two coordinates involved. The UXV readout structure (FIG. 1 (d)) is more complex considering its triangle arrangement of the sub-pixels that are connected along three symmetrical directions and form coordinate paths corresponding to the measurement channels. Hence, the algorithm is more elaborate[16].

In any case, however, for an intense radiation there are multi-hit events that are lost for histogramming. This is due to the fact that simultaneous photons could affect the same chain of connected pixels even being absorbed at different places on the readout plane. That brings ambiguity to the processing of such a multi-hit event. A possible solution would be to have smaller *and* independent pixels for unambiguous photon position/energy reconstruction. This, however, may not be practical as thousands are needed for good spatial resolution for even relatively small detecting surface.

C. Intense photon flux tests

As an example, charge distribution at different flux values on the UXV readout is presented in FIG. 3 for ~5 keV photons. The irradiated area was limited to ~100 mm^2 to restrict the total induced current in the detector volume and, thus, to insure stability of the applied high voltage to the detector electrodes. The maximum photon intensity was kept to provide the stable operation of the detector in terms of space charge effect for about 10^4 effective gain, so below ~0.1MHz/mm^2[10]. As the measured by GEM detector X-ray intensity deviates from linear relation at higher currents (starting from ~50 μA) it was validated independently by a commercial detector.

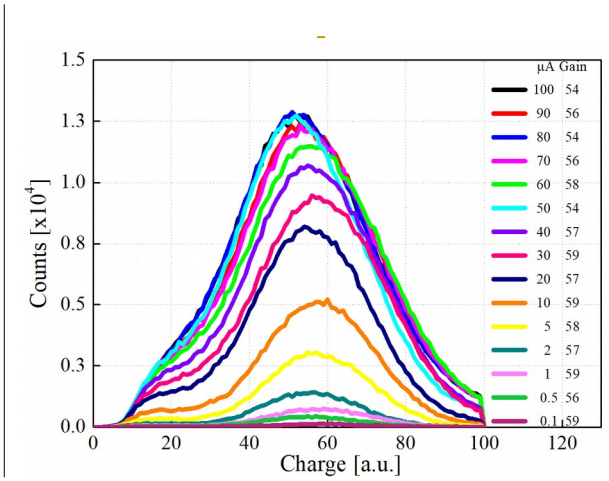

FIG. 3. Charge distribution at different flux values in the triple GEM detector with UXV readout structure irradiated by X-ray generator supplied at 5 kV. In the legend, X-ray generator current is given

In order to determine the considered readout structure limits for unambiguous determination of the photon produced charge and its position on the anode plane, this type of measurements was performed for all the readout structures. The results are presented in FIG. 4 along with the extrapolated X-ray generator rate. Such an extrapolation was done using measurements of the full range of the X-ray generator currents (intensities) by XR-100SDD AMPTEK detector under a condition of keeping small dead time (less than 2.4%), i.e. lower photon intensity (up to 3.2 kHz/mm^2). Afterwards, the lowest measured by GEM detector photon rate was used to scale the SDD detector results and to extrapolate the expected rate on the GEM detector at a given current of the generator. All the readout structures were tested under the same settings of the X-ray generator, slightly different in the resultant total flux on each readout due to minor changes of the geometrical set-up.

Looking at FIG. 4, it is seen that some fraction (marked as error bars) of all the recorded events will be rejected from further data processing. These include irregular charge clusters, ambiguous events when signals

of neighboring pixels coincide in time or in space, or the events that cannot be unambiguously resolved (exploiting at least one common coordinate/channel for separate events). Out of these unaccountable events, one can identify the fraction of the events that contain multiple-valued information due to interconnection between pixels. In case of the hexagonal pixels, for example, interconnection between pixels is absent and, therefore, rejected counts are dominantly related to the events that occur on the same pixel. For this anode, gathering higher rate information is at the expense of poorer spatial resolution at the reasonable?? electronics readout resources.

An observed deviation of the measured photon flux from the expected one, i.e. from the extrapolated one, is a sign that the overlapping of the collected signals and simultaneous coincidence rise for the irradiated area with the X-ray intensity growth. It should be also mentioned that the larger number of the incoming photons, the more overlapped signals are and the larger underestimation of the detection losses is, as more than two photons could generate a signal within the same readout channel. This could explain a difficulty to achieve exactly the extrapolated rate by summing the regular and rejected counts for the upper incoming radiation intensity.

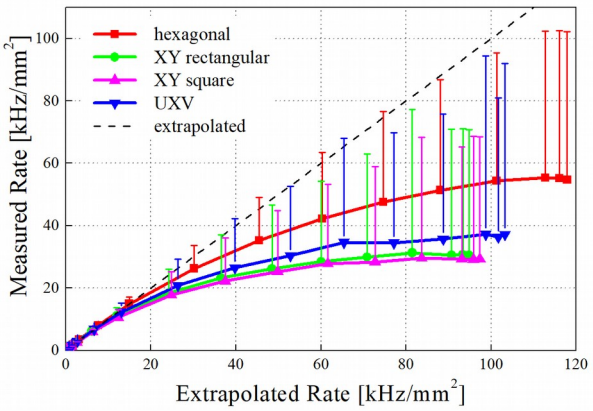

FIG. 4. Deviation of the GEM detector measured photon flux from the extrapolated X-ray intensity for all the readout structures. Total number of unaccountable events is marked as error bars. Extrapolated flux (grey dashed line) was obtained from the independent verification of the X-ray generator linearity by XR-100

Comparison of the results for such structures (UXV, XY rectangular and XY square) shows that they all suffer to an extent (above ~50%) from the lost information above 60kHz/mm^2 flux. Nevertheless, the slightly more effective detection within the measured photon flux was provided by UXV readout. Even the total amount of the rejected signals for UXV is quite close to the one for other two interconnected anodes, the wrong impression could be made as this readout is less matched to the cluster size at intense radiation, e.g. an amount of one-pixel clusters, whose position could not be defined, grows quicker for UXV compared to the XY readouts, 22% vs. 18 and 15% (in relation to the total amount of signals gathered for each structure at the maximal measured rate) for rectangular and square pixels, respectively. As only regular events (able to be resolved in time and space) allow defining the amount of cluster forming signals from different channels, all the rejected information relates to the total number of the acquired signals (single coordinate/electronics channel charges). Nevertheless, considering larger pixel for UXV structure comparing to two other interconnected readouts (that is higher probability of the signals/samples overlapping), it can handle higher throughput of the acquired signals resolution.

Since the tokamak plasma is a very bright SXR radiation source, it can produce a very intense photon flux on the detector surface achieving up to 10^5-10^7 photons·s^{-1}·mm^{-2}) depending on the heating power, impurities present in the plasma and the detector arrangement. Taking into account that tokamak plasma imaging of high spatial resolution would require enormous number of pixels directly connected to electronics readout channels, thus more appropriate would be to develop the readout with the reduced independent electronics paths. Therefore, for the plasma imaging purposes, UXV readout structure could be considered as quite promising basing configuration of the anode electrodes. Although, its photon rate capability might not be sufficient for the final application. Thus, a further research might be considered that will be aimed to optimize the patterned anode, e.g. decreasing the pixel size to get rid of single pixel clusters and to decrease the clusters overlapping. Adjusting in this case the cluster size by higher detector amplification (higher high voltages applied) is irrelevant as it limits the upper photon flux down.

D. Spatial resolution results

The spatial resolution is another important factor in imaging capabilities of detectors. Identification of the detector resolution function should ideally be performed via a conventional method. Barrier methods such as the narrow slot, the blade edge imaging[19], and/or pinhole imaging are also available, where several measured distributions are collected for different geometrical arrangements of source/barrier/detector. These measured distributions then are treated mathematically to obtain the desired function.

Here, first of all, the relative detector resolution for all the mentioned anode configurations was verified in measurements with the X-ray generator and long (50 mm) collimator with a pinhole of 1.1 mm diameter, both rigidly attached to the optical platform with the micrometric screw. The detector signals were collected in each of the source-pinhole chain positions shifted by 0.1 mm step. The results of the obtained photon spot position on the detector

readout are presented in for all four readout structures with the Gaussian fit to the measured spatial distribution of the photon beam. As can be observed, both XY readout structures keep a good correlation between measured and moved positions of the source. The hexagonal readout of independent pixels was found to be insensitive, as could be expected, to a small shift of the radiation source as its pixel size is much bigger than a single shift of the source position (0.1 mm).

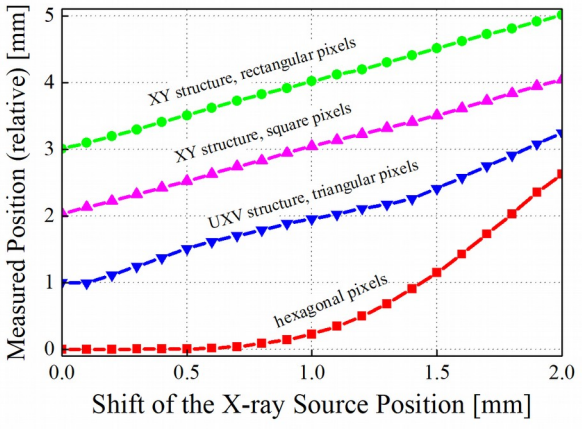

FIG. 5. Relative position resolution for all the readout structures.

An apparent nonlinearity in the measured positions for UXV readout comes from a cyclically granular readout structure. This makes the pixels more or less sensitive to the source shift. The extreme example is the coarse-grained hexagonal structure, where there are zones almost insensitive to the source movement. Some impact on the sensitivity to the source position is originated by a cluster charge range (accuracy/binning of data processing) that extends over several pixels and the size of the cluster relative to the pixel. For the presented tests, the cluster charge ranged to the maximal ADC sample values. That means that the detector being very sensitive to the small change in cluster location results in a recordable change of its charge distribution over the pixels. Nevertheless, this sensitivity varies locally depending on the location of the charge cluster relative to the pixels.

Finally, the spatial resolutions were obtained for each structure determining the point source spread functions and the Gaussian fit of the radiation image on the detector readout. The data were taken for ~6 keV photons generated by X-ray generator with the different positions of the irradiated spot (Ø1 mm) on the detecting surface. As can be expected and was observable in the tests with the shifts of the X-ray source (with the same parameters of the generator), the position distribution on the anode plane changes not only in location but also in shape (pixel arrangement), depending on the relative arrangement of the collimator and the readout structure. Therefore, the average distribution of the relative position, Y, (average shape) of all the source positions was calculated with its σ, the standard deviation of the Gaussian fit. The image is a convolution of point spread function (PSF), H, and half-ellipse, X, for a circular pinhole, which is a characteristic of a source with a collimator. The resulting image (position distribution Y) was estimated by Gaussian function. So, the convolution equation, $X * H = Y$, where H is an unknown PSF, was solved by matrix operations to obtain the PSF function and to calculate the width of this distribution. The results are collected in Table I.

TABLE I. Calculated spatial resolutions with their errors for the investigated readout structures.

GEM readout structure	Spatial resolution (mm)	Accuracy (mm)
Hexagonal pixels readout	3.40	0.10
XY squared pixels readout	0.96	0.03
XY rectangular pixels readout	1.02	0.03
UXV triangle pixels readout	1.17	0.06

The presented results give an estimation of the spatial resolution of the proposed anode arrangements. Among the examined readout structures with dependent electrodes, taking into account the rate capability results, it could be concluded that UXV based layout has some potential for effective and precise imaging of SXR plasma radiation and could serve as a base for further optimizations of the readout configuration.

III. CONCLUSIONS

Detection system based on the GEM technology has been proposed for tomographic and imaging plasma diagnostics with energy discrimination of plasma radiation. Imaging capabilities of different patterned anode planes (i.e. different readouts) of the Triple-GEM detector were preliminarily tested for SXR imaging. Under intense photon flux (~0.1 MHz/mm^2), hexagonal structure and structures with interconnected electrodes were found to fail to account for up to 50 and 65-70 % of the incoming signals, respectively. The best unambiguity in photon position/energy determination was found for UXV structure (20%) compared to the other two (34%). Having similar spatial resolution and accuracy (except the hexagonal structure), UXV based layout could be considered as a quite promising base of the anode electrodes configuration for plasma imaging. Currently, the photon rate capability might not be sufficient for the final application, thus, a further research is needed aimed to optimize the patterned anode in terms of cluster-pixel size relation, interconnected electrodes density, unambiguity of the readout layout, etc.

ACKNOWLEDGMENTS

This work has been carried out within the framework of the EUROfusion Consortium and has received funding from the Euratom research and training programme 2014-2018 under grant agreement No 633053. The views and opinions expressed herein do not necessarily reflect those of the European Commission. This scientific work was partly supported by Polish Ministry of Science and Higher Education within the framework of the scientific financial resources in the years 2014-2018 allocated for the realization of the international co-financed project.

[1]F. Sauli, Nucl. Instrum. Meth. A **805**, 2 (2016).
[2]M. Chernyshova et al., Fusion Eng. Des. **123**, 877 (2017).
[3]D. Mazon et al., Fusion Eng. Des. **96**, 856 (2015).
[4]M. Chernyshova et al., Rev. Sci. Instrum. **87**, 325 (2016).
[5]A. Jardin et al., JINST **11**, C07006 (2016).
[6]D. Mazon et al., JINST **11**, C08006 (2016).
[7]M. Chernyshova et al., JINST **10**, P10022 (2015).
[8]A. Karadzhinova et al., JINST **10**, P12014 (2015).
[9]O. Bouianov et al., Nucl. Instr. Meth. A **458**, 698 (2001).
[10]M. Chernyshova et al., Fusion Eng. Des., https://doi.org/10.1016/j.fusengdes.2018.03.031, accepted for publication (2018).
[11]A. Wojenski et al., Nucl. Instrum. Meth. B **364**, 49 (2015).
[12]A. Wojenski et al., Fusion Sci. Technol. **69**, 595 (2016).
[13]A. Wojenski et al., JINST **11**, C11035 (2016).
[14]A. Bressan et al., Nucl. Instrum. Meth. A **424**, 321 (1999).
[15]S. Bachmann et al., Nucl. Instrum. Meth. A **478**, 104 (2002).
[16]T. Czarski et al., Nucl. Instr. Meth. B **364**, 54 (2015).
[17]T. Czarski et al., Rev. Sci. Instrum. **87**, 11E336 (2016).
[18]T. Czarski et al., JINST **10**, P10013 (2015).
[19]X.-Y. Lu et al., Chinese Phys. C **36**, 228 (2012).